Supplementary Information

Directed exfoliating and ordered stacking of transition-metal-dichalcogenides

Yanshuang Li[1,2], Xiuhua Xie[1*], Binghui Li[1], Xiaoli Sun[3*], Yichen Yang[4], Jishan Liu[4,5*], Jiying Feng[6], Ying Zhou[6], Yuanzheng Li[6], Weizhen Liu[6], Shuangpeng Wang[7], Wei Wang[7], Huan Zeng[1,2], Zhenzhong Zhang[8], Dezhen Shen[1*]

[1]State Key Laboratory of Luminescence and Applications, Changchun Institute of Optics, Fine Mechanics and Physics, Chinese Academy of Sciences, No. 3888 Dongnanhu Road, Changchun, 130033, People's Republic of China

[2]University of Chinese Academy of Sciences, Beijing 100049, People's Republic of China

[3]Institute of Theoretical Chemistry, Jilin University, Changchun 130023, People's Republic of China

[4]Center for Excellence in Superconducting Electronics, State Key Laboratory of Functional Materials for Informatics, Shanghai Institute of Microsystem and Information Technology, Chinese Academy of Sciences, Shanghai 200050, China

[5]Center of Materials Science and Optoelectronics Engineering, University of Chinese Academy of Sciences, Beijing 100049, China

[6]Key Laboratory of UV-Emitting Materials and Technology, Ministry of Education, Northeast Normal University, Changchun 130024, China

[7]MOE Joint Key Laboratory, Institute of Applied Physics and Materials Engineering and Department of Physics and Chemistry, Faculty of Science and Technology, University of Macau, Macao SAR 999078, P. R. China

[8]School of Microelectronics, Dalian University of Technology, Dalian, 116024 China

*Corresponding authors. Email: xiexh@ciomp.ac.cn; sunxiaoli@jlu.edu.cn; jishanliu@mail.sim.ac.cn; shendz@ciomp.ac.cn

Supplementary Note 1: Scanning Electron Microscopy (SEM) images of gold (Au) crystal grains on the surface of MoS_2 bulk crystals.

MoS_2 bulk crystals were transferred on the surface of silicon. Then we grew thin Au atoms on the surface of MoS_2 bulk crystals by using molecular beam epitaxy (MBE). As shown in Supplementary Figure S1, Au atoms preferentially grow along the terrace edges of MoS_2 bulk crystals. Generally, Au nanocrystals grew in a triangular shape and aligned along the side of each triangle. Supplementary Figure S1c shows the minority situation that Au grains grow along two perpendicular directions. The line arranged along the angle bisector of the triangle is along with the armchair (AC) direction. In Supplementary Figure S1d, the side of Au triangles mainly arrange along the edges of hexagon, which means that the steps are along zigzag (ZZ) directions. In other locations, there is a few Au triangles. It indicates that Au atoms preferentially grow along ZZ edges of MoS_2 after the initial stage of epitaxy.

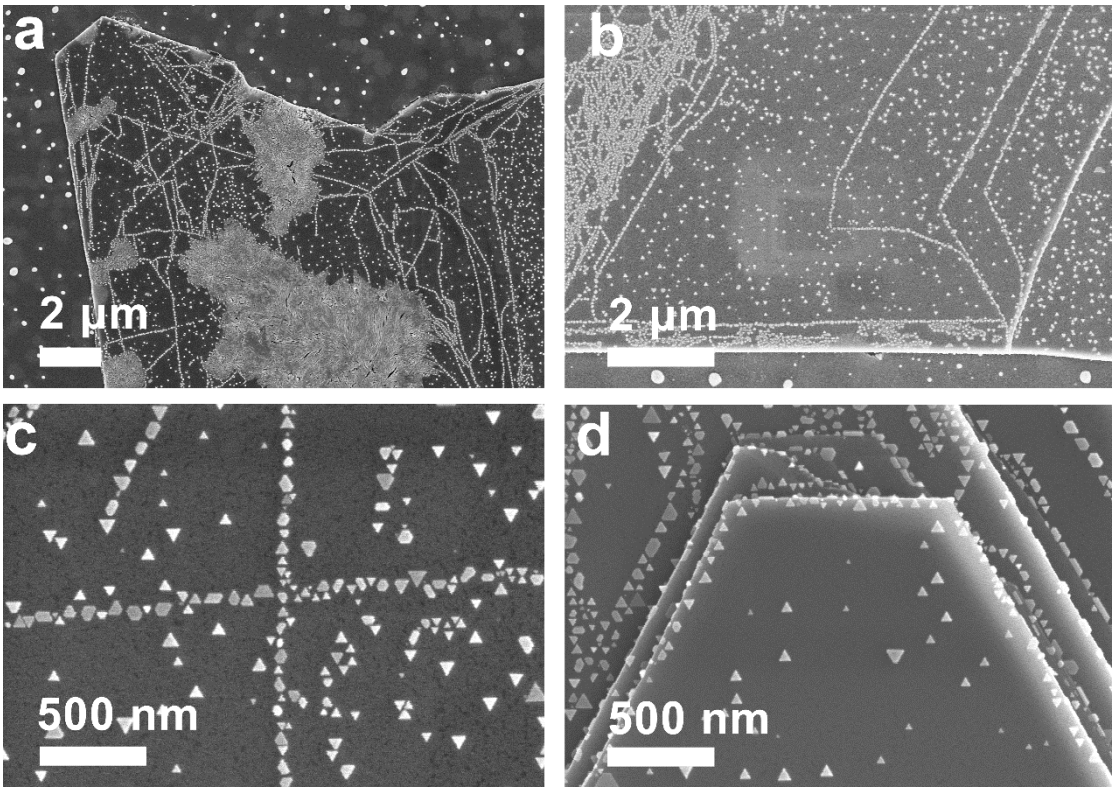

Supplementary Figure S1 | a and **b**, Au grains along terrace edges of MoS_2. **c**, Au grains along zigzag and armchair two directions perpendicular to each other, and **d**, along zigzag directions of hexagon MoS_2.

Supplementary Note 2: Second harmonic generation (SHG) and optical images of transition metal dichalcogenides (TMDs).

We obtained monolayer WS_2, $MoSe_2$, and WSe_2 by Au-assisted mechanical exfoliation and made SHG testing. Because the intensity of polarization-dependent SHG is related to the crystalline symmetry, AC edges are the direction with the strongest signal. For these monolayer TMDs, the long straight edges are AC directions. So we could distinguish the AC directions by the long straight edges between monolayer and multilayer.

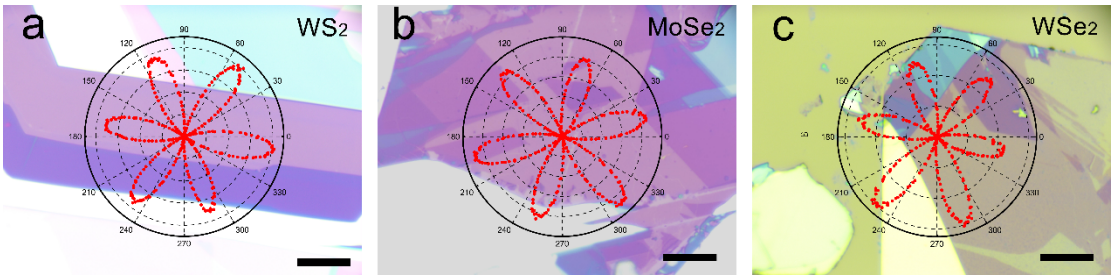

Supplementary Figure S2 | a-c, The straight edges of TMDs coincide with the strongest direction of the SHG. And it indicates that it is the armchair direction. Scale bars, 10 μm. (a) WS_2, (b) $MoSe_2$, (c) WSe_2.

Supplementary Note 3: Photoluminescence Spectroscopy (PL) and Raman spectra of monolayers including $MoSe_2$, WS_2, and WSe_2.

The emission peak of $MoSe_2$ is 793 nm (1.56 eV). The Raman peaks of in-plane E^1_{2g} mode and out-of-plane A_{1g} mode of $MoSe_2$ are 288.1 and 240.4 cm^{-1}. And the spacing between the two peaks is about 47.7 cm^{-1}. The above two points suggest that the Au-assisted mechanical exfoliation $MoSe_2$ is a monolayer. Similarly, the emission peaks of WS_2 and $MoSe_2$ are 623 nm (1.99 eV) and 746 nm (1.66 eV), respectively. Correspondingly， the spacing between the two E^1_{2g} and A_{1g} peaks are 64.9 and 14.7 cm^{-1}. These suggest that the Au-assisted mechanical exfoliation WS_2 and WSe_2 are also monolayers.

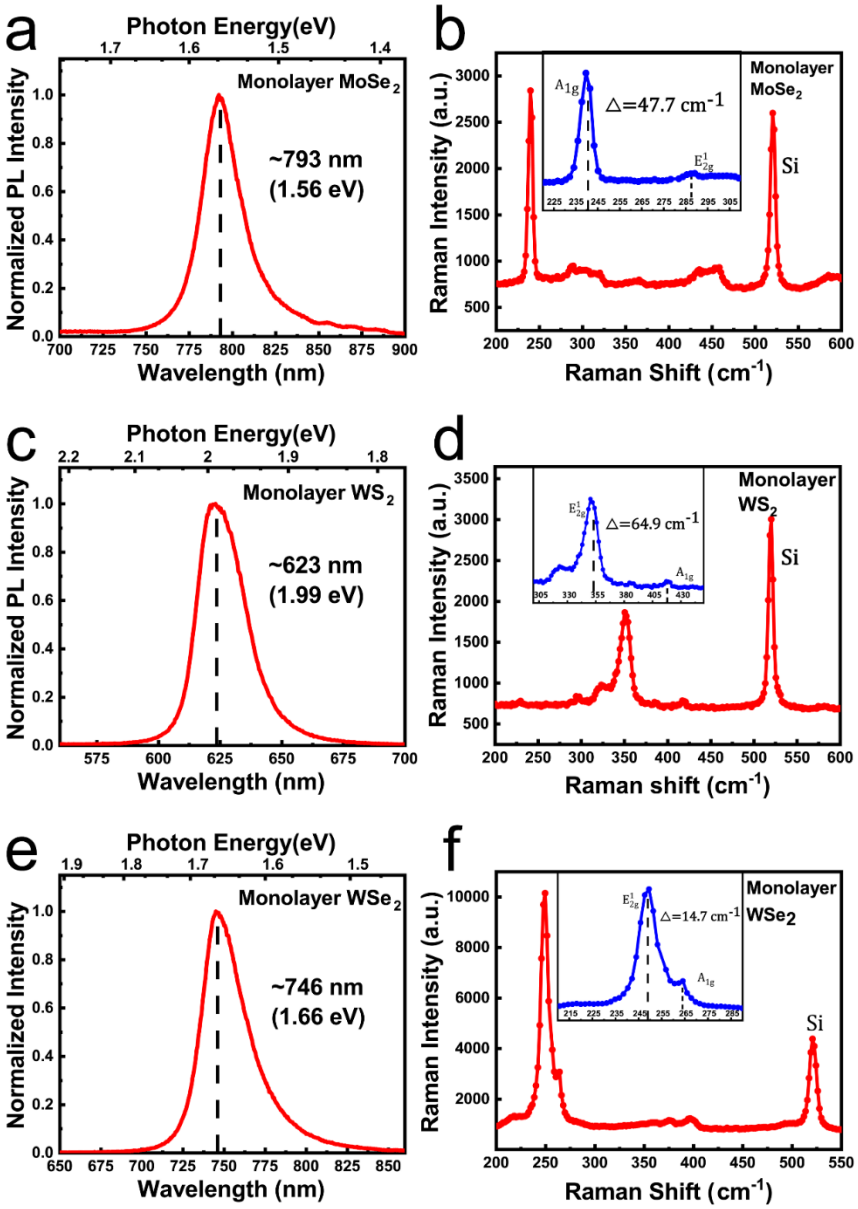

Supplementary Figure S3 | a-f, PL and Raman of monolayers are carried out at room temperature with excitation laser wavelength 532.18 nm. (a)(c)(e) Normalized PL spectra intensity of monolayer $MoSe_2$, WS_2, and WSe_2. (b)(d)(f) Raman peaks of in-plane E^1_{2g} mode and out-of-plane A_{1g} mode of monolayer $MoSe_2$, WS_2, and WSe_2.

Supplementary Note 4: PL and Raman spatial mapping of monolayer MoS_2.

In PL mapping, the dominant emission peak of MoS_2 is 660 nm. While the spacing between two E^1_{2g} and A_{1g} peaks is also less than 20 cm^{-1} in Raman mapping. The uniform distribution of PL peak wavelength and Raman mode spacing indicates that Au-assisted mechanical exfoliation monolayer MoS_2 has good uniformity and high crystal quality.

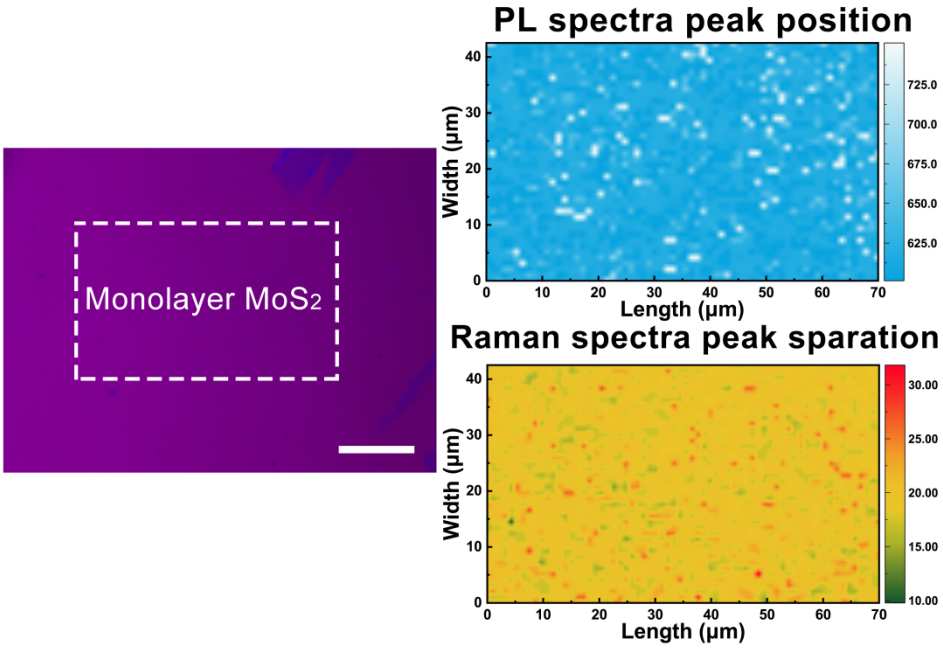

Supplementary Figure S4 | a, Optical image of monolayer MoS_2 testing areas (white dotted rectangle) on Si/SiO_2 (285 nm) surface. The scale bar is 20 μm. **b**, PL spatial mapping of emission peak wavelength and **c**, Raman spatial mapping of peak separation between in-plane E^1_{2g} mode and out-of-plane A_{1g} are also performed at room temperature with excitation laser wavelength 532.18 nm.

Supplementary Note 5: Optical images of mechanical exfoliation MoS_2 and WS_2 on gold surface.

We grew Au atoms by MBE and direct current sputtering (DCS) both on MoS_2 and WS_2 bulk crystals. Then we obtain monolayer and multilayer MoS_2 and WS_2 on Au films. Unlike fully surface relaxation combining Au with Mo atoms along ZZ edges by MBE, Au atoms quickly deposited on the surface of MoS_2 and WS_2 crystals by DCS. The faster deposition process makes it that Au atoms difficult to catch the terrace edges of MoS_2 and WS_2 bulk crystals. We could find that the MoS_2 and WS_2 edges of monolayer and bilayer are clear and sharp by MBE compared to DCS. In addition, it is difficult to obtain large-area monolayers by DCS. So, the key of Au-assisted mechanical exfoliation is slowly growing Au atoms by MBE.

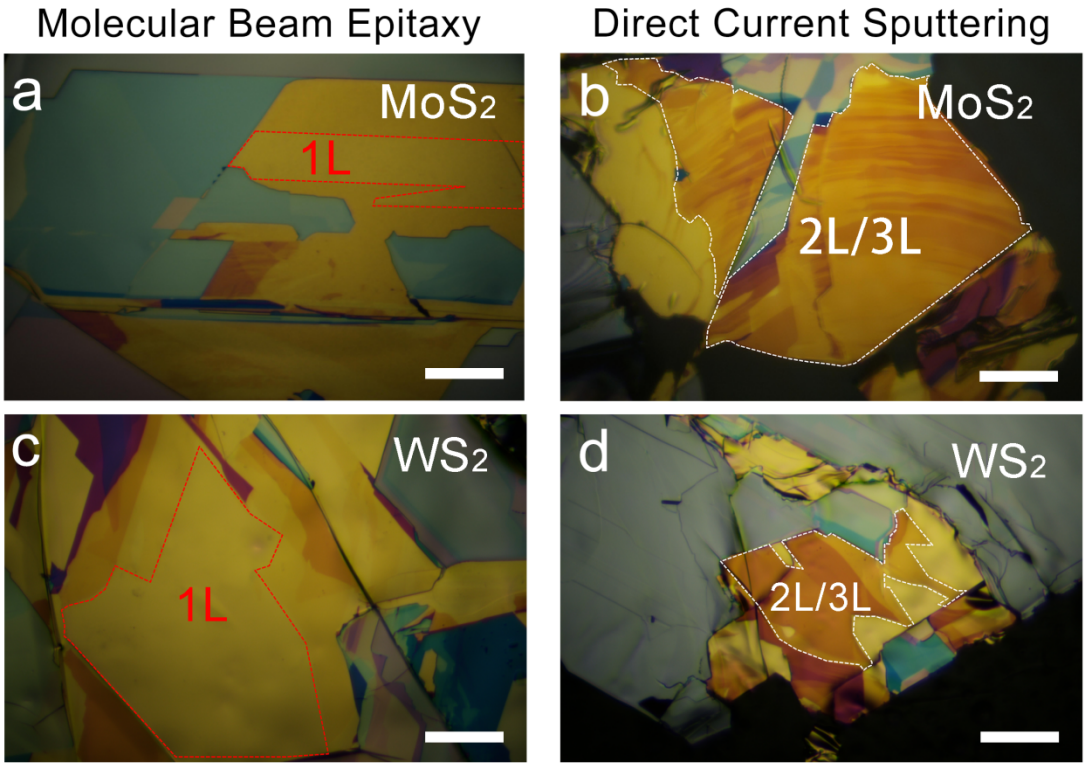

Supplementary Figure S5 | a and **c**, Clearly zigzag edges and large areas of monolayer MoS_2 and WS_2 with epitaxy gold by MBE. **b** and **d**, Not clearing edges and small areas of monolayer MoS_2 and WS_2 with sputtering gold. Scale bars, 50 μm.

Supplementary Note 6: Statistical results of the area and straight edges of monolayers

We obtained 65 monolayer MoS_2 on Au films. Then we counted the area and the ratio of directional straight edges (AC direction) in perimeter of monolayer MoS_2. We found that all monolayer area is over 10000 μm^2 and the average ratio of AC in perimeter is about 25%. These indicate that we could reproducibly obtain large area and directional monolayers of TMDs by our Au-assisted oriented mechanical exfoliation method.

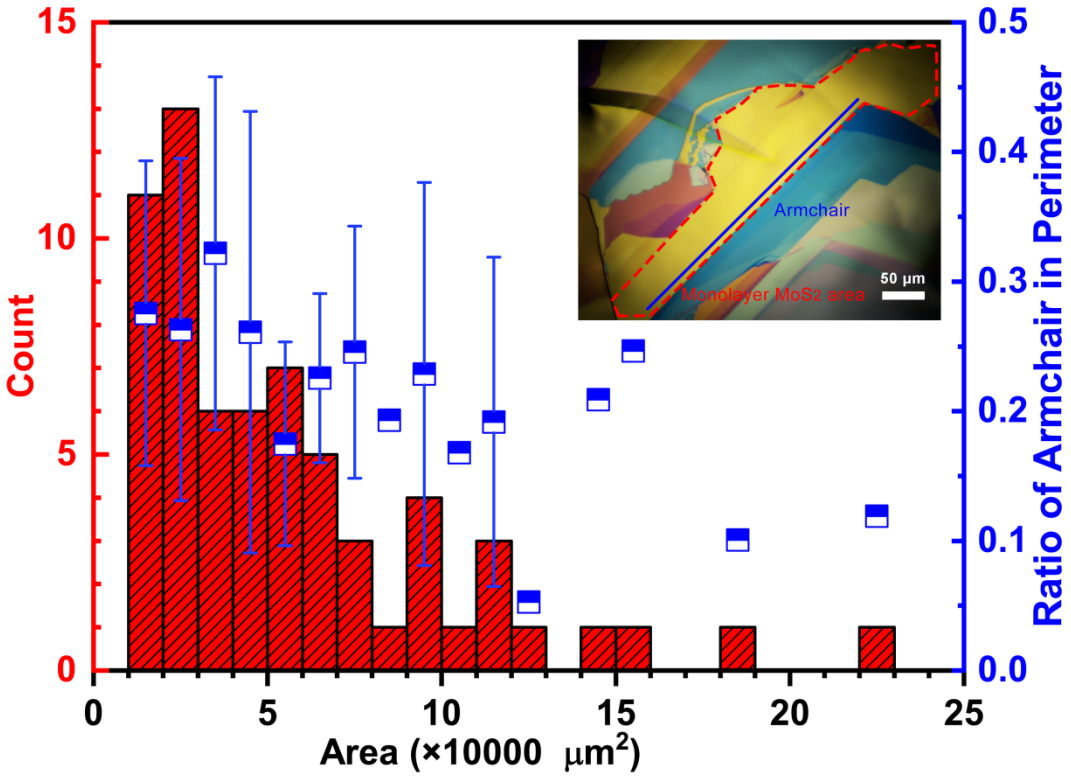

Supplementary Figure S6 | Histogram of large areas monolayer MoS_2 film and the rate of armchair slid to the perimeter. In monolayer MoS_2 with an area of more than 10000 um^2, the most ratio is above 0.2.

Supplementary Note 7: Artificial stacking process for H- and R-type symmetry.

In Supplementary Figure S7a, the long straight tearing edges are AC directions. Because Au atoms prefer to bonded Mo atoms along ZZ atomic step edges, the monolayer exfoliation direction is from ZZ-Mo to ZZ-S side along with AC directions. Equally, we could distinguish lattice orientation in Figure S7b, which monolayer is on polydimethylsiloxane (PDMS). Then we complete H-type stacking by aligning the two AC edges on PDMS and Si/SiO_2 (285 nm) with making ZZ-Mo (Fig. S7a) and ZZ-S (Fig. S7b) on the same side. Compared to H-type stacking, R-type stacking is opposite, namely, ZZ-Mo (Fig. S7d) and ZZ-Mo (Fig. S7e) on the same side.

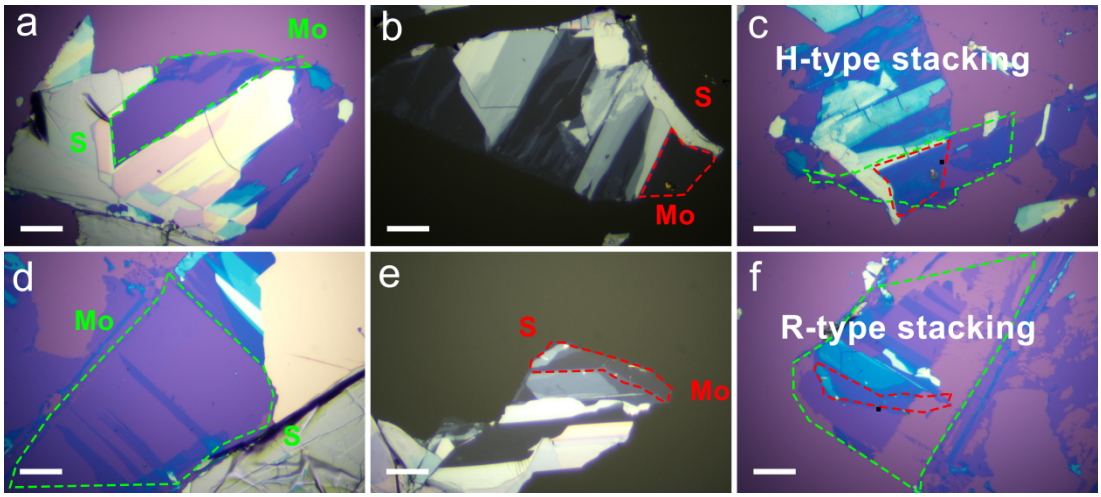

Supplementary Figure S7 | a-f, Schematic illustration of MoS_2 stacking directions. (a), (b), and (c) is H-type stacking. (d), (e), and (f) is R-type stacking. Scale bars, 50 μm.

Supplementary Note 8: DFT Calculations and Model establishment.

The definition and formula for ε, E_s, E_d, and E_c are as follows,

$\varepsilon = E_c/L$

$E_s = E_s(Au\text{-}MoS_2) – E(Au) - E_s(MoS_2)$

$E_d = E_d(Au\text{-}MoS_2) – E(Au) - E_d(MoS_2)$

$E_c = E_d - E_s = E_d(Au\text{-}MoS_2) - E_s(Au\text{-}MoS_2) - E_d(MoS_2) + E_s(MoS_2)$

Here, E(Au) and $E(MoS_2)$ are the energies of separate gold substrate and MoS_2 slab in Fig. 2. This is also the definition in other TMDs.

The optimized lattice constant of WS_2, $MoSe_2$, and WSe_2 are 3.18, 3.32 and 3.32 Å respectively, which is in good agreement with the experimental values of 3.154, 3.288 and 3.292 Å[1-3]. The establishment of Au(111)-WS_2 is the same as that of Au(111)-MoS_2. The Au(111)-$MoSe_2$ and Au(111)-WSe_2 overlayer were modeled by a ($8\sqrt{3}$ × $7\sqrt{3}$) Au(111) on ($7\sqrt{3}$ × $6\sqrt{3}$) $MoSe_2$ or WSe_2 bilayer to simulate the contact configurations between Au edges and $MoSe_2$ or WSe_2 substrate with a lattice mismatch of ~3.3%.

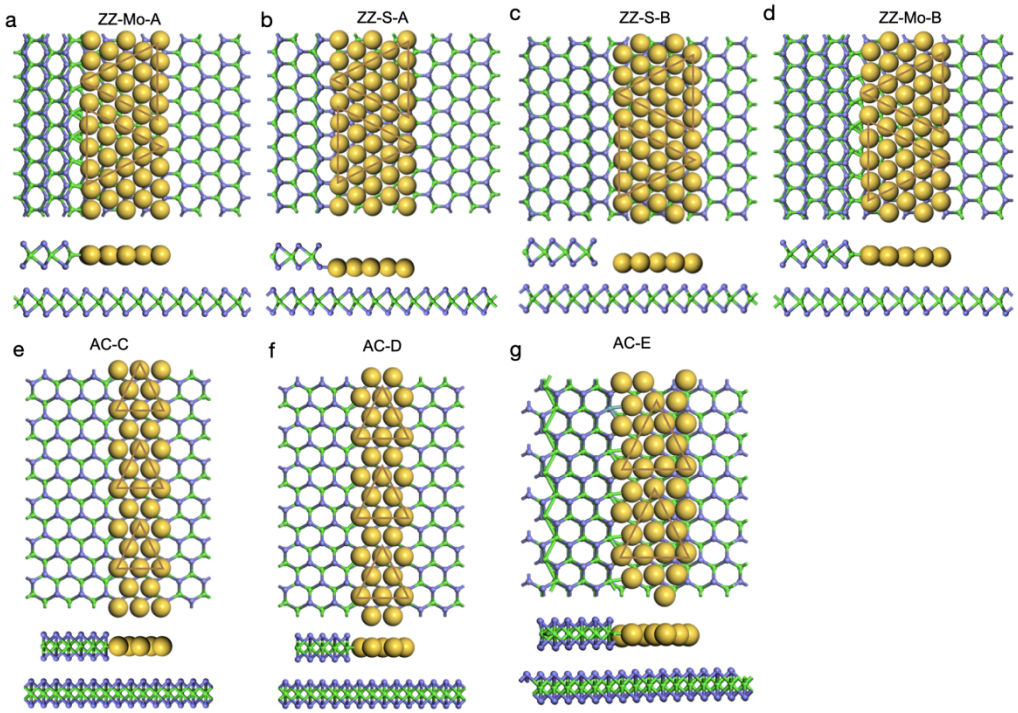

Supplementary Figure S8 | The ⟨110⟩ direction on Au(111) surface along two typical MoS_2 step edges and the ⟨112⟩ direction on Au(111) surface along one typical MoS_2 step edge. Atoms in golden, green and blue colors represent the Au, Mo and S atoms, respectively. **a**, **b**, coincide with Zigzag direction (ZZ-Mo and ZZ-S) with A step; **c**, **d**, coincide with Zigzag direction (ZZ-Mo and ZZ-S) with B step; **e**, **f**, armchair (AC) direction with C and D steps. **g**, armchair (AC) directions, Au (111)-MoS_2 overlayer were modeled by a ($9\sqrt{3}$ × $5\sqrt{3}$) Au(111) on ($8\sqrt{3}$ × $5\sqrt{3}$) MoS_2 bilayer to simulate the contact configurations.

Supplementary Note 9: Etching MoS_2 by water solution of hydrogen peroxide.

In Supplementary Figure S9, we use water solution of hydrogen peroxide (volume ratio H_2O: H_2O_2=3:17) to etch MoS_2. The black arrows mark the exfoliating direction. Along AC edge direction, the S atoms were etched. In Figure S9b, the multilayer AC edges were obviously etched. Compared to AC edges, the ZZ edges did not change significantly. It indicates that exfoliating direction

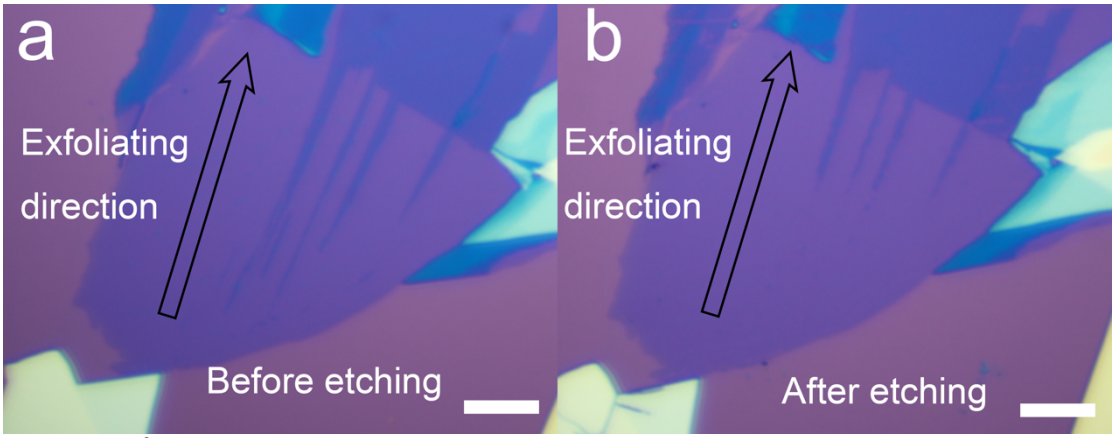

Figure S9 | MoS_2 optical images of before and after etching by water solution of hydrogen peroxide a, Before etching; b, After etching. Scale bars, 30 μm.

Supplementary Note 10: Each step of exfoliating MoS_2 and compared experiments.

In Supplementary Figure S10, we show every step of the Au-assisted mechanical exfoliation. In Supplementary Figure S11, we did three other compared experiments.，which showed the importance of controlling the Au flux by MBE.

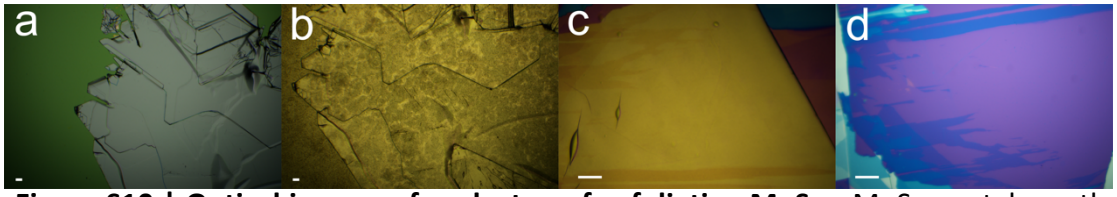

Figure S10 | Optical images of each step of exfoliating MoS_2 a,MoS_2 crystals on the substrate; b, Epitaxy Au by MBE; c, Monolayer MoS_2 on the surface of Au and thermal release tape. d, Monolayer MoS_2 was transferred on SiO_2/Si substrate. Scale bars, 30 μm.

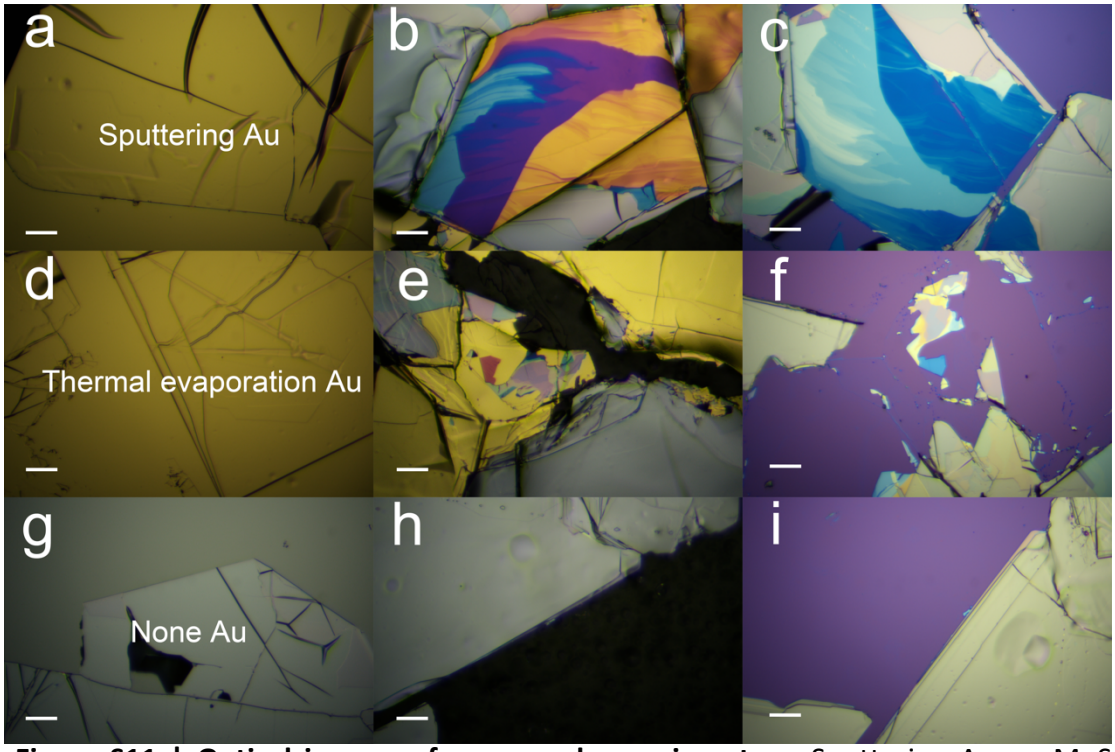

Figure S11 | Optical images of compared experiments a, Sputtering Au on MoS_2 crystals on substrate; d, Thermal evaporation Au on MoS_2 crystals on substrate; g, None Au on MoS_2 crystals on substrate; b, e, h Multilayer MoS_2 on the surface of Au and thermal release tape. c, f, i, Multilayer MoS_2 were transferred on SiO_2/Si substrate. Scale bars, 30 μm.

Supplementary Note 11: PL spectra of MoS_2/WS_2 bilayer heterostructure.

In Supplementary Figure S12, we show typical PL spectrum of interlayer excitons in a MoS_2/WS_2 heterostructure compared with the spectra of the constituent monolayers. The distinct PL signal of interlayer excitons further illustrates that the monolayer exfoliated based on our method has a relatively clean surface, and thus stronger interlayer coupling can be obtained.

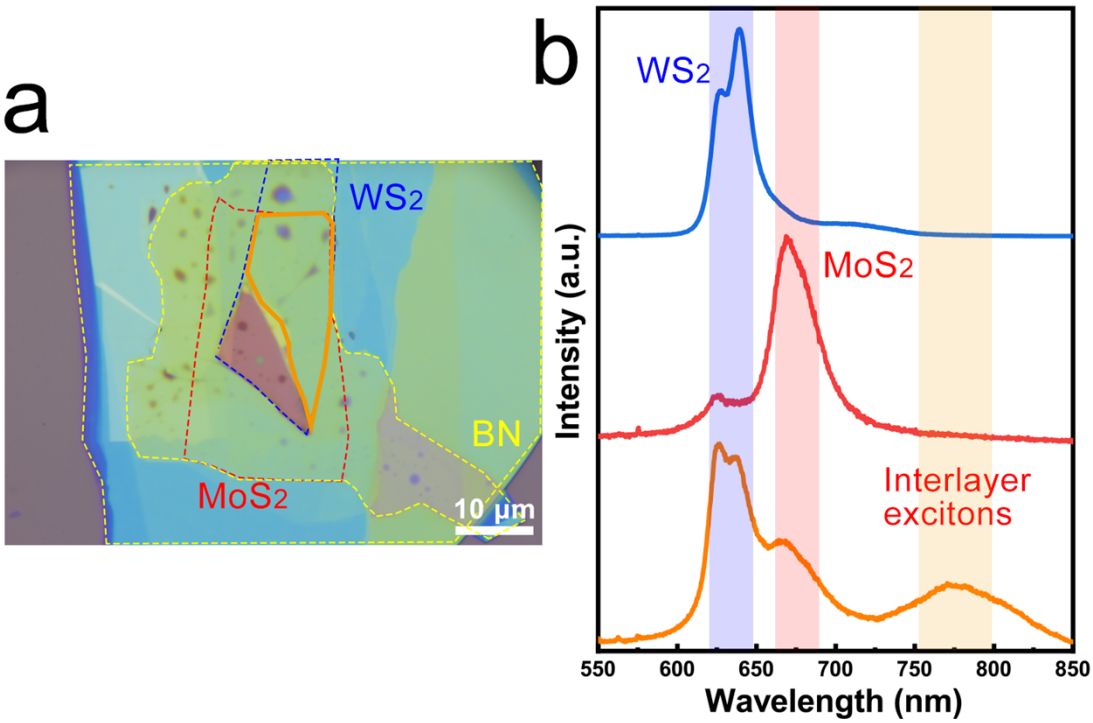

Supplementary Figure S12| a, Mechanically stacked MoS_2/WS_2 heterobilayers encapsulated by hBN. b, PL spectrum of interlayer excitons in a MoS_2/WS_2 heterostructure (orange line) compared with the spectra of the constituent monolayers (blue line and red line).

Supplementary Table 1

Step contact energies per unit of the length of edges between the three edges of MoS_2, WS_2, $MoSe_2$, WSe_2 step and Au(111), respectively.

ε (eV/Å)	MoS_2	WS_2	$MoSe_2$	WSe_2
ZZ-M	-1.11	-0.81	-0.68	-0.66
ZZ-Chalcogen	-0.19	-0.11	-0.40	-0.37
AC	-0.64	-0.68	-0.55	-0.51

Reference:

1. Wilson, J., Yoffe, A. The transition metal dichalcogenides discussion and interpretation of the observed optical, electrical and structural properties. *Adv. Phys.* 1969, **18**, 193.

2. Bromley, R. A., Murray, R. B., Yoffe, A. D. The band structures of some transition metal dichalcogenides. III. Group VIA: trigonal prism materials. *J. Phys. C: Solid State Physics* 1972, **5**, 759-778.

3. Kumar, A., Ahluwalia, P. K. Electronic structure of transition metal dichalcogenides monolayers 1H-MX_2 (M = Mo, W; X = S, Se, Te) from ab-initio theory: new direct band gap semiconductors. *Eur. Phys. J. B* 2012, **85**, 186.